Constraints on Dark Matter Microphysics from the Milky Way Satellite Population

Ethan O. Nadler[1], Vera Gluscevic[2,3], Kimberly K. Boddy[4], and Risa H. Wechsler[1,5]

[1] Kavli Institute for Particle Astrophysics and Cosmology and Department of Physics, Stanford University, Stanford, CA 94305, USA; enadler@stanford.edu
[2] Department of Physics and Astronomy, University of Southern California, Los Angeles, CA 90089-0484, USA
[3] Joseph Henry Laboratories of Physics, Jadwin Hall, Princeton University, Princeton, NJ 08544, USA
[4] Department of Physics & Astronomy, Johns Hopkins University, Baltimore, MD 21218, USA
[5] SLAC National Accelerator Laboratory, Menlo Park, CA 94025, USA

Abstract

Alternatives to the cold, collisionless dark matter (DM) paradigm in which DM behaves as a collisional fluid generically suppress small-scale structure. Herein we use the observed population of Milky Way (MW) satellite galaxies to constrain the collisional nature of DM, focusing on DM–baryon scattering. We first derive conservative analytic upper limits on the velocity-independent DM–baryon scattering cross section by translating the upper bound on the lowest mass of halos inferred to host satellites into a characteristic cutoff scale in the linear matter power spectrum. We then confirm and improve these results through a detailed probabilistic inference of the MW satellite population that marginalizes over relevant astrophysical uncertainties. This yields 95% confidence upper limits on the DM–baryon scattering cross section of 6×10^{-30} cm^2 (10^{-27} cm^2) for DM particle masses m_χ of 10 keV (10 GeV); these limits scale as $m_\chi^{1/4}$ for $m_\chi \ll 1$ GeV and m_χ for $m_\chi \gg 1$ GeV. This analysis improves upon cosmological bounds derived from cosmic-microwave-background anisotropy measurements by more than three orders of magnitude over a wide range of DM masses, excluding regions of parameter space previously unexplored by other methods, including direct-detection experiments. Our work reveals a mapping between DM–baryon scattering and other alternative DM models, and we discuss the implications of our results for warm and fuzzy DM scenarios.

Key words: cosmology: theory – dark matter – galaxies: halos – methods: numerical

1. Introduction

In the standard cold, collisionless dark matter (CDM) paradigm, structure forms from initial conditions described by a featureless power spectrum of matter perturbations, giving rise to a present-day dark matter (DM) halo mass function that extends uninterrupted down to sub-solar masses (Green et al. 2004; Diemand et al. 2005). Non-standard DM scenarios, such as warm DM (WDM; Abazajian 2017; Adhikari et al. 2017) and fuzzy DM (FDM; Hu et al. 2000; Hui et al. 2017), often involve smoothing of matter perturbations and suppression of structure on small scales.

Herein we focus on the framework inspired by the weakly interacting-massive-particle paradigm, in which DM scatters with Standard Model particles (i.e., baryons), through a velocity-independent contact interaction. These interactions transfer heat and momentum between the photon–baryon and DM fluids in the early universe, and damp matter perturbations on scales that enter the cosmological horizon while scattering is efficient (e.g., Boddy & Gluscevic 2018). The damping scale is set by the interaction strength, and the cumulative effect is largest for the smallest modes, which spend the most time inside the horizon.

As perturbations grow, this distinct fingerprint of DM microphysics is propagated to visible tracers of matter throughout cosmic history as a suppression of small-scale structure relative to CDM. Currently, the best cosmological limits on DM–baryon scattering come from measurements of damping tails in the cosmic-microwave-background (CMB) temperature and polarization power spectra from *Planck* (Boddy & Gluscevic 2018; Gluscevic & Boddy 2018; Xu et al. 2018) and the Lyα forest flux power spectrum from the Sloan Digital Sky Survey (SDSS; Dvorkin et al. 2014; Xu et al.

2018; Ooba et al. 2019). Moving beyond probes of quasi-linear cosmological perturbations, the suppression imprinted on the matter power spectrum at early times leads to an underabundance of collapsed objects—notably, low-mass DM halos in our Galactic neighborhood, and the faint galaxies that reside within them. As low-mass halos arise from matter fluctuations on scales far smaller than those captured by the CMB and other high-redshift probes, population studies of nearby dwarf galaxies could deliver dramatic improvements in sensitivity to DM–baryon interactions.

In this work, we analyze the observed population of Milky Way (MW) satellite galaxies to place stringent limits on velocity-independent DM–baryon elastic scattering.[6] We present both a conservative analytic derivation of these limits and a rigorous likelihood analysis in which we marginalize over uncertainties related to the connection between galaxies and halos and the impact of baryonic physics on subhalo abundances. Our population analysis yields 95% confidence upper limits on the DM–baryon scattering cross section of $(6 \times 10^{-30}, 2 \times 10^{-29}, 7 \times 10^{-29}, 10^{-27})$ cm^2 for DM particle masses of $(10^{-5}, 10^{-3}, 10^{-1}, 10)$ GeV, improving upon CMB limits by more than three orders of magnitude (see Figure 1). This analysis probes unexplored regions of DM parameter space, and it is complementary to direct-detection constraints that rely on the local DM distribution.

This Letter is organized as follows: in Section 2, we derive conservative analytic limits on DM–baryon scattering from the existence of low-mass halos; in Section 3, we present our

---

[6] We consider DM–proton interactions, and therefore constrain both the spin-independent and spin-dependent DM–nucleon scattering cross section. Because we neglect helium, our constraints for spin-independent scattering are conservative for DM masses above ∼1 GeV (Boddy et al. 2018).
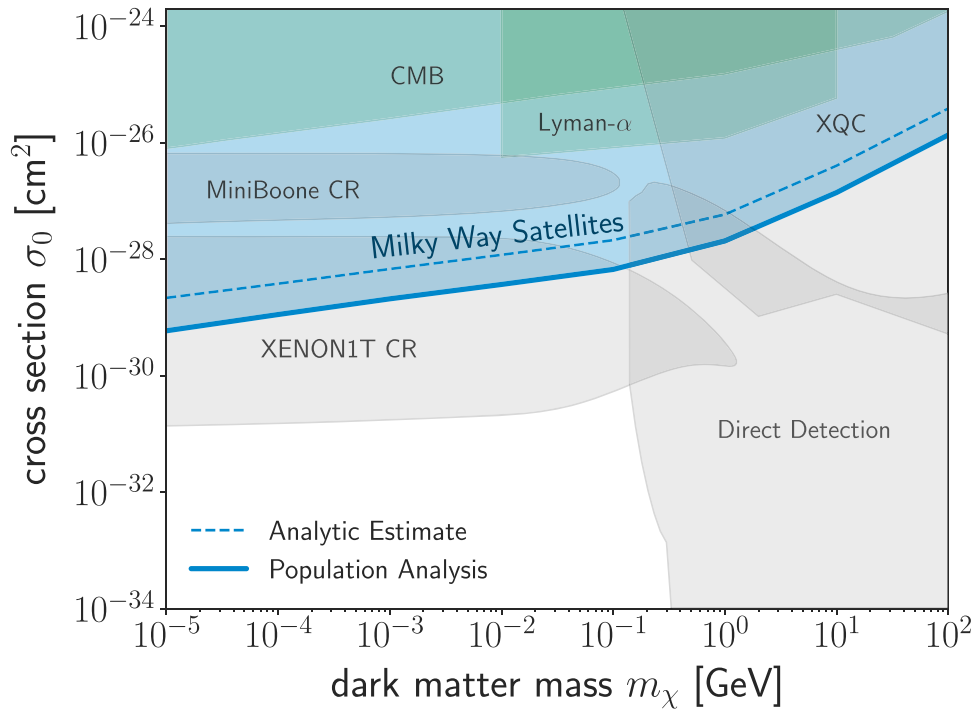
Figure 1. Upper limits on the velocity-independent DM–proton scattering cross section as a function of DM particle mass. The blue shaded region is excluded by the population of classical and SDSS-discovered MW satellites with 95% confidence by our likelihood analysis, which marginalizes over relevant astrophysical uncertainties (Section 3). The dashed line shows a conservative analytic upper limit derived from the existence of the lowest-mass halos hosting satellites (Section 2). Green contours show cosmological constraints from the CMB (Boddy & Gluscevic 2018; Gluscevic & Boddy 2018) and the Lyα forest (Xu et al. 2018). Gray contours show experimental constraints from cosmic-ray scattering (Bringmann & Pospelov 2019), the X-ray Quantum Calorimeter (XQC; Erickcek et al. 2007), and direct-detection experiments including CRESST-III (CRESST Collaboration et al. 2017), the CRESST 2017 surface run (Angloher et al. 2017), and XENON1T (Aprile et al. 2017), as interpreted by Emken & Kouvaris (2018). Limits from Galactic center gas clouds (Bhoonah et al. 2018; Wadekar & Farrar 2019) overlap with parts of the XQC, CMB, and Lyα contours for 10^{-3} GeV $\lesssim m_\chi \lesssim$ 100 GeV, and are omitted for clarity.

likelihood analysis of the MW satellite population and the corresponding DM–baryon scattering limits; in Section 4, we translate our results into constraints on other non-CDM models; we discuss caveats and conclude in Section 5. Throughout, we adopt the best-fit *Planck* cosmology with Hubble parameter $h = 0.6727$, DM density $\Omega_m h^2 = 0.1199$, and baryon density $\Omega_b h^2 = 0.0222$ (Planck Collaboration et al. 2016), and we set $c = k_B = 1$.

2. Analytic Estimate from Individual Halos

To develop physical intuition for the effects of DM–baryon interactions on the late-time population of DM halos, we first derive an analytic estimate for the mass of the smallest halo allowed to form in an interacting cosmology.[7] We then translate upper limits on the minimum halo mass into upper limits on the DM–baryon scattering cross section. The limits we obtain in this Section are conservative and do not depend strongly on observational completeness corrections or on galaxy–halo connection modeling, as demonstrated in Section 2.2.

2.1. Minimum Halo Mass in an Interacting Cosmology

In a non-standard cosmology with DM–baryon interactions, linear matter perturbations smaller than a critical length scale $\lambda_{\rm crit} = 2\pi/k_{\rm crit}$ are substantially suppressed relative to CDM. As the universe expands, collision damping affects

progressively larger scales; when scattering becomes inefficient, the DM and baryon fluids kinetically decouple. The size of the largest perturbation entirely erased by DM collisions corresponds to the size of the cosmological horizon when the rate of momentum transfer R_χ between the DM and baryon fluids drops below the Hubble rate aH

$$aH = R_\chi|_{z=z_{\rm crit}}, \tag{1}$$

where $z_{\rm crit}$ is the corresponding redshift. To calculate $z_{\rm crit}$, we use the expression for the velocity-averaged momentum transfer rate for velocity-independent DM–proton scattering (Boddy & Gluscevic 2018)

$$R_\chi = \mathcal{N}_0 a \rho_b Y_p \frac{\sigma_0}{m_\chi + m_p}\left(\frac{T_b}{m_p} + \frac{T_\chi}{m_\chi}\right)^{1/2}, \tag{2}$$

where $\mathcal{N}_0 \equiv 2^{7/2}/(3\sqrt{\pi})$; a is the scale factor; ρ_b is the baryon energy density; Y_p is the proton mass fraction; σ_0 is the velocity-independent DM–proton scattering cross section; m_χ is the DM particle mass; m_p is the proton mass; and T_b and T_χ are the temperatures of the baryon and DM fluids, respectively. The term $(T_b/m_p + T_\chi/m_\chi)^{1/2}$ is the thermal dispersion of the relative velocity between the DM and baryon fluids. At early times, the interactions keep the fluids in thermal equilibrium. In particular, the heat transfer rate $R'_\chi \equiv (m_\chi/(m_\chi + m_p))R_\chi$ exceeds the Hubble rate, driving the DM temperature to that of the photon–baryon fluid, $T_\chi = T_b = T_0 (1 + z)$, where T_0 is the CMB temperature today. Thermal decoupling occurs at $z_{\rm th}$,

---

[7] Note that Boehm et al. (2001) and Boehm & Schaeffer (2005) perform similar derivations for DM–photon and DM–neutrino scattering models.
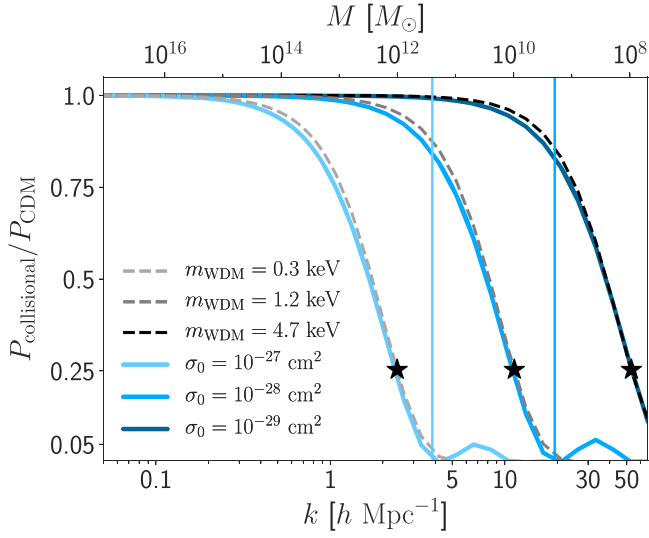
Figure 2. Ratio of the linear matter power spectrum in a DM–baryon scattering cosmology to that in CDM (solid lines), for a range of interaction cross sections (for 1 MeV DM particles). Dashed lines show the same quantity for WDM models with matching half-mode scales (denoted as black stars). Vertical lines indicate the critical scale discussed in Section 2.

when the heat transfer rate decreases sufficiently, such that

$$aH = R'_\chi|_{z=z_{\text{th}}}. \qquad (3)$$

Note that z_{th} occurs deep within the radiation-dominated era, when $H \approx H_0 \sqrt{\Omega_{\text{rad}}} z^2$, where $\Omega_{\text{rad}} \approx 10^{-4}$ is the radiation energy density divided by the critical density today, $\bar{\rho}$. After thermal decoupling ($z < z_{\text{th}}$), DM cools adiabatically and $T_\chi = T_0 (1+z)^2/(1+z_{\text{th}})$.

Solving Equation (3) for z_{th}, accounting for the thermal evolution of the DM and baryon fluids in Equation (2), and making appropriate substitutions in Equation (1), we can find z_{crit} given the parameters σ_0 and m_χ that describe our DM–baryon scattering model. Next, requiring the critical mode to undergo a full oscillation within the cosmological horizon, we compute the corresponding wavenumber k_{crit} via

$$k_{\text{crit}} = 2\left(\frac{1}{aH}\right)^{-1}\bigg|_{z=z_{\text{crit}}}. \qquad (4)$$

Modes with $k > k_{\text{crit}}$ in the linear matter power spectrum are extremely suppressed (see Figure 2).

The next step is to determine the mass of a collapsed halo arising from perturbation modes that correspond to k_{crit}. For this purpose, we use the relation

$$M_{\text{crit}} = \frac{4\pi}{3}\rho_m\left(\frac{\lambda_{\text{crit}}}{2}\right)^3 = \frac{4\pi}{3}\Omega_m\bar{\rho}\left(\frac{\pi}{k_{\text{crit}}}\right)^3. \qquad (5)$$

Combining with Equation (4), this yields

$$M_{\text{crit}}(\sigma_0, m_\chi) \approx \frac{\pi^4}{6}\frac{(\mathcal{N}_0 Y_p \Omega_b)^2\Omega_m\bar{\rho}^3}{(H_0\sqrt{\Omega_{\text{rad}}})^5}\frac{T_0}{m_p}\left(\frac{\sigma_0}{\widetilde{m}_\chi}\right)^2, \qquad (6)$$

where $\widetilde{m}_\chi$ asymptotes to m_χ for $m_\chi \gg m_p$ and to $(m_\chi m_p^3)^{1/4}$ for $m_\chi \ll m_p$; the expression for intermediate DM mass does not have a closed form. Halos that are less massive than $M_{\text{crit}}(\sigma_0, m_\chi)$ do not form in a cosmology with DM–

baryon interactions because power vanishes on the corresponding scales due to early-time scattering.

2.2. Limits on the Interaction Cross Section

If halos are detected down to a minimum mass M_{min}, interpreting an upper limit on M_{min} as an upper limit on M_{crit} yields an upper bound on σ_0, at fixed m_χ. This bound is very conservative because the power spectrum is severely suppressed at k_{crit}. Thus, detecting a single halo with $M < M_{\text{crit}}$ confidently excludes cross sections that correspond to k_{crit}.

Many independent astrophysical probes testify to the existence of low-mass halos and set upper limits on M_{min}. For example, substructure detections in strongly lensed systems (Vegetti et al. 2012; Hezaveh et al. 2016b) and the dynamical masses of dwarf galaxies obtained from spectroscopy (e.g., Simon et al. 2011) both imply that halos exist down to a mass of $\sim 10^9 M_\odot$. Recent studies of the MW satellite population that model the galaxy–halo connection, completeness corrections of observed satellites, and the impact of baryonic physics on galaxy formation and subhalo abundances have pushed the upper bound on M_{min} even lower. For example, Nadler et al. (2019) report $M_{\text{min}} < 5.4 \times 10^8 M_\odot$ with 95% confidence using classical and SDSS-discovered MW satellites, and Jethwa et al. (2018) derived consistent results. These studies do not include ultra-faint satellites discovered in recent years (Bechtol et al. 2015; Drlica-Wagner et al. 2015, 2016; Koposov et al. 2015, 2018; Laevens et al. 2015a, 2015b; Homma et al. 2016); accounting for these systems will further improve limits on M_{min}. In addition, upcoming surveys including the Large Synoptic Survey Telescope (LSST; LSST Science Collaboration et al. 2009) are expected to discover even more faint MW satellites, which could lower M_{min} by a factor of ~ 5 compared to current constraints (Drlica-Wagner et al. 2019).

The observed MW satellite population likely contains several halos that are near the current limit on the minimum halo mass. Thus, we set $M_{\text{crit}} < 5.4 \times 10^8 M_\odot$ to derive a very conservative bound of $k_{\text{crit}} > 30 \, h \, \text{Mpc}^{-1}$. Using this scale in our analytic prescription yields $\sigma_0 < 2 \times 10^{-29} \, \text{cm}^2$ for a DM particle mass of 10 keV. Constraints for other DM particle masses are shown in Figure 1.

It is important to note that these limits scale weakly with M_{min}. In particular, the upper limit on σ_0 scales as $M_{\text{crit}}^{1/2}$, so increasing M_{min} by an order of magnitude only weakens the limit on σ_0 by a factor of ~ 3. Thus, these constraints do not depend sensitively on the galaxy–halo connection and completeness correction modeling used to derive M_{min}, and they shift by small amounts if halo masses obtained from strong lensing or spectroscopic measurements are instead chosen as the reference.

3. Satellite Population Likelihood Analysis

Halo formation is affected at masses well above M_{crit} due to the gradual power suppression caused by DM–baryon interactions (see Figure 2). Thus, using a *population* of low-mass halos should yield more stringent limits than the existence of a single low-mass halo. In this section, we therefore perform a probabilistic analysis of the MW satellite population to place more realistic constraints on DM–baryon scattering; our results are shown in Figure 1.

In principle, accounting for the detailed effects of DM–baryon scattering on the late-time halo population requires

simulations that self-consistently include both the initial linear power suppression described above as well as late-time DM–baryon interactions. However, we find that the power suppression in the DM–baryon scattering case is remarkably similar to that in WDM, as shown in Figure 2. Moreover, we expect late-time interactions to be a small effect for the interaction model that we consider. Taken together, these facts allow us to use the results of WDM simulations run with nearly identical initial conditions as the DM–baryon scattering model under consideration.

To derive the correspondence between DM–baryon scattering and WDM, we use a modified version of the Boltzmann solver CLASS (described in Boddy & Gluscevic 2018; Boddy et al. 2018; Gluscevic & Boddy 2018), which evolves linear cosmological perturbations in the presence of DM–baryon interactions. We generate linear matter power spectra as a function of σ_0 and m_χ, and we compare these to WDM power spectra using the transfer function in Schneider et al. (2012) by matching the *half-mode scale* k_{hm}, i.e., the wavenumber at which the transfer function $T(k) = (P_{collisional}(k)/P_{CDM}(k))^{1/2}$ is equal to 50%. We compute $k_{hm}(\sigma_0, m_\chi)$ numerically using our Boltzmann solver by varying σ_0 at several values of m_χ.

The correspondence shown in Figure 2 allows us to map the suppression in MW subhalo abundances found in WDM simulations to our interacting cosmology. In particular, we use the subhalo mass function from Lovell et al. (2014), which is fit to cosmological zoom-in simulations of thermal relic sterile neutrino WDM

$$\frac{dN}{dM}\bigg|_{collisional} = \frac{dN}{dM}\bigg|_{CDM} \left(1 + \gamma \frac{M_{hm}}{M}\right)^{-\beta}, \qquad (7)$$

where $\gamma = 2.7$, $\beta = 0.99$, M is the peak subhalo virial mass output by the halo finder, and M_{hm} is the mass corresponding to k_{hm} via a relation equivalent to Equation (5).

Next, to forward-model the MW satellite population, we modify the framework presented in Nadler et al. (2019). In particular, we supplement high-resolution DM-only simulations of MW-mass host halos (Mao et al. 2015) with a flexible model for the galaxy–halo connection and the impact of both baryonic physics and DM–baryon scattering on subhalo populations. We then fit the luminosity function of classical and SDSS-discovered MW satellites using a Poisson likelihood in bins of satellite luminosity. As in Nadler et al. (2019), free parameters in our fit include the slope and scatter in the galaxy–halo connection and the strength of subhalo disruption due to baryonic effects. These are nuisance parameters with large uncertainties that should be marginalized over for the purpose of placing robust limits on DM microphysics. We use the ratio of the collisional-to-CDM subhalo mass functions in Equation (7) to assign a "survival probability" to each subhalo in our CDM simulations, following Jethwa et al. (2018). Thus, the final free parameter in our fit is M_{hm}, and we obtain a marginalized posterior distribution $P(M_{hm})$ using a flat prior on $\log(M_{hm})$. To be conservative, we assume that *all* subhalos host galaxies, even though the galaxy occupation fraction is likely low and mass-dependent in this regime (e.g., Sawala et al. 2016; Fitts et al. 2018). A non-trivial occupation fraction could force lighter subhalos to host observed satellites, further strengthening our constraints. However, we find that marginalizing over a step-function galaxy formation threshold does not significantly affect our results.

Finally, we map $P(M_{hm})$ to $P(\sigma_0|m_\chi)$ using our half-mode scale calculation. We find $M_{hm} < 3.1 \times 10^8 M_\odot$ (corresponding to $k_{hm} > 36\,h\,\mathrm{Mpc}^{-1}$) with 95% confidence, yielding upper limits on σ_0 of $(6 \times 10^{-30}, 2 \times 10^{-29}, 7 \times 10^{-29}, 10^{-27})\,\mathrm{cm}^2$ for DM particle masses of $(10^{-5}, 10^{-3}, 10^{-1}, 10)$ GeV, as shown in Figure 1. These limits improve upon CMB constraints by more than three orders of magnitude for $m_\chi \lesssim 1$ GeV, and can be extrapolated to higher masses. However, for $m_\chi \lesssim 10$ keV, relativistic effects become important. Moreover, in the following section we show that thermal DM lighter than ~ 3 keV is ruled out at all cross sections.

4. Implications for Other Non-CDM Models

The methods developed in this work apply to *any* model in which DM behaves similarly to a collisional fluid on small scales. For example, we can translate our M_{hm} constraint to a lower limit on WDM mass by combining the transfer function derived in Schneider et al. (2012) for a thermal relic sterile neutrino of mass m_{WDM} with the half-mode mass equivalent of Equation (5), which yields

$$m_{WDM} = 2.32 \left(\frac{\Omega_m}{0.25}\right)^{0.4} \left(\frac{h}{0.7}\right)^{0.8} \left(\frac{M_{hm}}{10^9 M_\odot}\right)^{-0.3} \mathrm{keV}. \quad (8)$$

We find $m_{WDM} > 3.26$ keV with 95% confidence, which is consistent with previous MW satellite results (Jethwa et al. 2018) and competitive with Lyα forest constraints (Viel et al. 2013; Iršič et al. 2017b).

Our results also constrain FDM models, in which ultra-light axions comprise DM and small-scale structure is suppressed due to quantum interference effects (Hu et al. 2000; Hui et al. 2017). We translate our M_{hm} constraint into a lower limit on FDM mass m_ϕ using the m_{WDM}–m_ϕ relation from Armengaud et al. (2017) in Equation (8), which gives

$$m_\phi = 1.3 \times 10^{-21} \left(\frac{\Omega_m}{0.25}\right)^{0.95} \left(\frac{h}{0.7}\right)^{1.9} \left(\frac{M_{hm}}{10^9 M_\odot}\right)^{-0.71} \mathrm{eV}. \quad (9)$$

We find $m_\phi > 2.9 \times 10^{-21}$ eV, which is again competitive with Lyα forest constraints (Iršič et al. 2017a). We note that the high-redshift galaxy luminosity function and the epoch of reionization provide WDM and FDM constraints that are complementary to—but currently weaker than—our limits (e.g., Corasaniti et al. 2017).

We expect that a re-analysis of the MW satellite population using our method will yield even more stringent limits for velocity-dependent DM–baryon scattering, i.e., for any scattering model in which the cross section scales as the relative particle velocity to a positive power. Such interactions arise in DM effective theory (e.g., Boddy & Gluscevic 2018), and we leave an investigation of this scenario to future work.

5. Conclusions and Discussion

Small-scale tracers of the matter distribution in the universe provide insights into DM microphysics that are complementary to other probes. In this work, we report stringent upper bounds on DM–baryon scattering for a velocity-independent contact interaction by analyzing the population of classical and SDSS-discovered MW satellite galaxies. Based on the consistency of the satellite population with CDM expectations down to a halo

mass scale of $\sim 10^8 M_\odot$, we place robust limits on a range of DM interaction cross sections and particle masses. Our analysis closes unexplored gaps in DM–baryon scattering parameter space, improving upon previous cosmological bounds by several orders of magnitude, and it is not subject to uncertainties in the local DM distribution or cosmic-ray propagation.

In our likelihood analysis, we have accounted for several astrophysical uncertainties, including the slope and scatter of the low-mass galaxy–halo relation and the impact of baryonic physics on subhalo abundances. We have made the conservative assumption that *all* subhalos host galaxies, though marginalizing over a step-function galaxy formation threshold does not affect our results. Moreover, Nadler et al. (2019) verified that potential spurious numerical effects in our simulations (e.g., artificial subhalo disruption) do not alter the inferred minimum halo mass.

There are several possible caveats to our analysis that we leave for future work. First, we have not investigated how our results depend on cosmological parameters. However, we expect uncertainties on cosmological parameters to play a minimal role; for example, Equation (6) implies that limits on σ_0 scale as $\Omega_m^{-1/2}$. Future analyses that marginalize over cosmological parameters are needed to confirm this weak dependence. Next, we relied on simulations with a narrow range of host halo mass, even though the uncertainty on the mass of MW is relatively large (e.g., Deason et al. 2019). We do not expect this uncertainty to affect our results significantly, as $M_{\min}$ scales linearly with host mass and our limits depend weakly on $M_{\min}$. To further improve our constraints, it will be necessary to understand how a mass-dependent galaxy occupation fraction and baryonic effects beyond enhanced subhalo disruption affect satellite populations in detail.

This work demonstrates that the MW satellite population places competitive constraints on a class of non-CDM models. Moreover, it paves the way for joint probabilistic analyses of forthcoming small-scale structure data sets. For example, upcoming imaging surveys such as LSST will facilitate systematic searches for density gaps in Galactic stellar streams, which potentially trace even lower-mass subhalos than those inferred from satellites (e.g., Bonaca et al. 2018). In addition, gravitational lensing measurements with the Atacama Large Millimeter/submillimeter Array will map out low-mass DM substructure in a complementary manner to faint galaxies (e.g., Hezaveh et al. 2016a). Finally, future spectroscopic surveys like DESI (DESI Collaboration et al. 2016) will provide improved Lyα forest measurements, allowing for important high-redshift consistency tests of local small-scale structure constraints. Distinct systematic and modeling uncertainties accompany each of these DM probes, and joint likelihood analyses of all available data sets—enabled by approaches similar to ours—will be crucial in order to study the nature of DM in the era of next-generation surveys.

ORCID iDs

Ethan O. Nadler ● https://orcid.org/0000-0002-1182-3825
Vera Gluscevic ● https://orcid.org/0000-0002-3589-8637
Kimberly K. Boddy ● https://orcid.org/0000-0003-1928-4667
Risa H. Wechsler ● https://orcid.org/0000-0003-2229-011X

References

Abazajian, K. N. 2017, PhR, 711-712, 1
Adhikari, R., Agostini, M., Ky, N. A., et al. 2017, JCAP, 1, 025
Angloher, G., Bauer, P., Bento, A., et al. 2017, EPJC, 77, 637
Aprile, E., Aalbers, J., Agostini, F., et al. 2017, PhRvL, 119, 181301
Armengaud, E., Palanque-Delabrouille, N., Yèche, C., Marsh, D. J. E., & Baur, J. 2017, MNRAS, 471, 4606
Bechtol, K., Drlica-Wagner, A., Balbinot, E., et al. 2015, ApJ, 807, 50
Bhoonah, A., Bramante, J., Elahi, F., & Schon, S. 2018, PhRvL, 121, 131101
Boddy, K. K., & Gluscevic, V. 2018, PhRvD, 98, 083510
Boddy, K. K., Gluscevic, V., Poulin, V., et al. 2018, PhRvD, 98, 123506
Boehm, C., Fayet, P., & Schaeffer, R. 2001, PhLB, 518, 8
Boehm, C., & Schaeffer, R. 2005, A&A, 438, 419
Bonaca, A., Hogg, D. W., Price-Whelan, A. M., & Conroy, C. 2018, arXiv:1811.03631
Bringmann, T., & Pospelov, M. 2019, PhRvL, 122, 171801
Corasaniti, P. S., Agarwal, S., Marsh, D. J. E., & Das, S. 2017, PhRvD, 95, 083512
CRESST collaboration, Petricca, F., Angloher, G., et al. 2017, arXiv:1711.07692
Deason, A. J., Frenk, C. S., Cautun, M., et al. 2019, MNRAS, 484, 5453
DESI Collaboration, Aghamousa, A., Aguilar, J., et al. 2016, arXiv:1611.00036
Diemand, J., Moore, B., & Stadel, J. 2005, Natur, 433, 389
Drlica-Wagner, A., Bechtol, K., Rykoff, E. S., et al. 2015, ApJ, 813, 109
Drlica-Wagner, A., Bechtol, K., Allam, S., et al. 2016, ApJ, 833, L5
Drlica-Wagner, A., Mao, Y.-Y., Adhikari, S., et al. 2019, arXiv:1902.01055
Dvorkin, C., Blum, K., & Kamionkowski, M. 2014, PhRvD, 89, 023519
Emken, T., & Kouvaris, C. 2018, PhRvD, 97, 115047
Erickcek, A. L., Steinhardt, P. J., McCammon, D., & McGuire, P. C. 2007, PhRvD, 76, 042007
Fitts, A., Boylan-Kolchin, M., Bullock, J. S., et al. 2018, MNRAS, 479, 319
Gluscevic, V., & Boddy, K. K. 2018, PhRvL, 121, 081301
Green, A. M., Hofmann, S., & Schwarz, D. J. 2004, MNRAS, 353, L23
Hezaveh, Y., Dalal, N., Holder, G., et al. 2016a, JCAP, 2016, 048
Hezaveh, Y. D., Dalal, N., Marrone, D. P., et al. 2016b, ApJ, 823, 37
Homma, D., Chiba, M., Okamoto, S., et al. 2016, ApJ, 832, 21
Hu, W., Barkana, R., & Gruzinov, A. 2000, PhRvL, 85, 1158
Hui, L., Ostriker, J. P., Tremaine, S., & Witten, E. 2017, PhRvD, 95, 043541
Iršič, V., Viel, M., Haehnelt, M. G., Bolton, J. S., & Becker, G. D. 2017a, PhRvL, 119, 031302
Iršič, V., Viel, M., Haehnelt, M. G., et al. 2017b, PhRvD, 96, 023522
Jethwa, P., Erkal, D., & Belokurov, V. 2018, MNRAS, 473, 2060
Koposov, S. E., Belokurov, V., Torrealba, G., & Evans, N. W. 2015, ApJ, 805, 130
Koposov, S. E., Walker, M. G., Belokurov, V., et al. 2018, MNRAS, 479, 5343
Laevens, B. P. M., Martin, N. F., Ibata, R. A., et al. 2015a, ApJL, 802, L18
Laevens, B. P. M., Martin, N. F., Bernard, E. J., et al. 2015b, ApJ, 813, 44
Lovell, M. R., Frenk, C. S., Eke, V. R., et al. 2014, MNRAS, 439, 300
LSST Science Collaboration, Abell, P. A., Allison, J., et al. 2009, arXiv:0912.0201
Mao, Y.-Y., Williamson, M., & Wechsler, R. H. 2015, ApJ, 810, 21
Nadler, E. O., Mao, Y.-Y., Green, G. M., & Wechsler, R. H. 2019, ApJ, 873, 34
Ooba, J., Tashiro, H., & Kadota, K. 2019, arXiv:1902.00826
Planck Collaboration, Ade, P. A. R., Aghanim, N., et al. 2016, A&A, 594, A13
Sawala, T., Frenk, C. S., Fattahi, A., et al. 2016, MNRAS, 456, 85
Schneider, A., Smith, R. E., Macciò, A. V., & Moore, B. 2012, MNRAS, 424, 684
Simon, J. D., Geha, M., Minor, Q. E., et al. 2011, ApJ, 733, 46
Vegetti, S., Lagattuta, D. J., McKean, J. P., et al. 2012, Natur, 481, 341

Viel, M., Becker, G. D., Bolton, J. S., & Haehnelt, M. G. 2013, PhRvD, 88, 043502

Wadekar, D., & Farrar, G. R. 2019, arXiv:1903.12190
Xu, W. L., Dvorkin, C., & Chael, A. 2018, PhRvD, 97, 103530

Erratum: "Constraints on Dark Matter Microphysics from the Milky Way Satellite Population" (2019, ApJL, 878, 32)

Ethan O. Nadler[1] , Vera Gluscevic[2,3] , Kimberly K. Boddy[4] , and Risa H. Wechsler[1,5]
[1] Kavli Institute for Particle Astrophysics and Cosmology and Department of Physics, Stanford University, Stanford, CA 94305, USA; enadler@stanford.edu
[2] Department of Physics and Astronomy, University of Southern California, Los Angeles, CA 90089-0484, USA
[3] Joseph Henry Laboratories of Physics, Jadwin Hall, Princeton University, Princeton, NJ 08544, USA
[4] Department of Physics & Astronomy, Johns Hopkins University, Baltimore, MD 21218, USA
[5] SLAC National Accelerator Laboratory, Menlo Park, CA 94025, USA
Received 2020 June 16; published 2020 July 15

The modified CLASS code used in the published article (Nadler et al. 2019, hereafter N19) contained an erroneous prefactor that enhanced the suppression of linear matter power spectra in our interacting dark matter (DM) model. With this prefactor removed, the corrected code yields power spectra that match those used in N19 if the original velocity-independent DM–proton scattering cross sections, σ_0, are increased by a factor of 4 (at all DM masses, m_χ).

We have verified that this correction increases the Milky Way (MW) satellite population analysis limits on σ_0 presented in N19 by a factor 4 at all DM masses. Thus, our 95% confidence population analysis upper limits on σ_0 become (2×10^{-29}, 8×10^{-29}, 3×10^{-28}, 6×10^{-27}) cm^2 for DM particle masses of (10^{-5}, 10^{-3}, 10^{-1}, 10) GeV, as shown in Figure 1. These limits improve upon cosmic-microwave-background (CMB) constraints by a factor of ∼300 for $m_\chi \lesssim 1$ GeV, rather than the factor of ∼1000 claimed in N19. We emphasize that both the shape of the cross section limit (i.e., its dependence on m_χ) and its qualitative interpretation are unchanged. Importantly, even with the correction, the limits presented in N19 exclude regions of DM–proton scattering parameter space previously unexplored by other methods, and improve upon previous cosmological bounds by multiple orders of magnitude.

The analytic cross section constraints presented in N19 did not depend on CLASS output and are therefore unaffected. However, the interpretation of the analytic limits changes because the power spectra returned by CLASS are now less suppressed at fixed σ_0 and m_χ. In particular, our analytic estimate of the minimum halo mass in the presence of DM–proton scattering now lies at a less
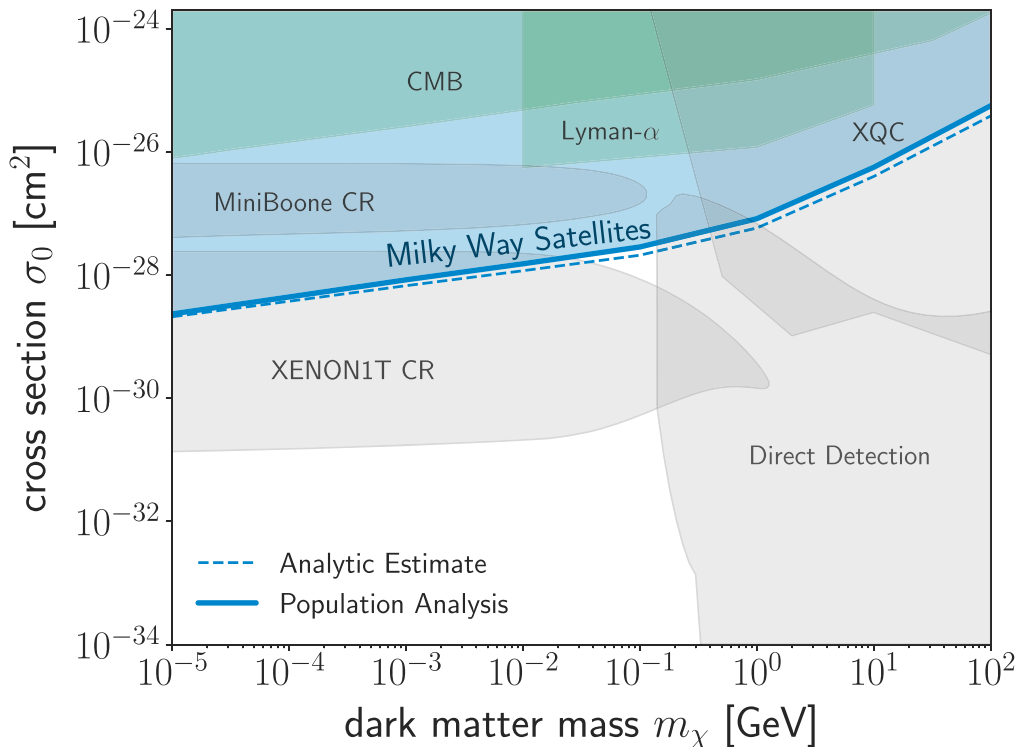

Figure 1. Upper limits on the velocity-independent DM–proton scattering cross section as a function of DM particle mass. The blue shaded region is excluded by the population of classical and SDSS-discovered MW satellites with 95% confidence by our population analysis. The dashed line shows an analytic upper limit derived from the existence of the lowest-mass halos hosting satellites. Green contours show cosmological constraints from the CMB (Boddy & Gluscevic 2018; Gluscevic & Boddy 2018) and the Lyα forest (Xu et al. 2018). Gray contours show experimental constraints from cosmic-ray scattering (Bringmann & Pospelov 2019), the X-ray Quantum Calorimeter (XQC; Erickcek et al. 2007), and direct-detection experiments including CRESST-III (Petricca et al. 2020), the CRESST 2017 surface run (Angloher et al. 2017), and XENON1T (Aprile et al. 2017), as interpreted by Emken & Kouvaris (2018). Limits from Galactic center gas clouds (Bhoonah et al. 2018; Wadekar & Farrar 2019) overlap with parts of the XQC, CMB, and Lyα contours for 10^{-3} GeV $\lesssim$ m$_\chi$ $\lesssim$ 100 GeV, and are omitted for clarity. The population analysis limits are a factor of 4 weaker than those presented in N19 at all DM particles masses.
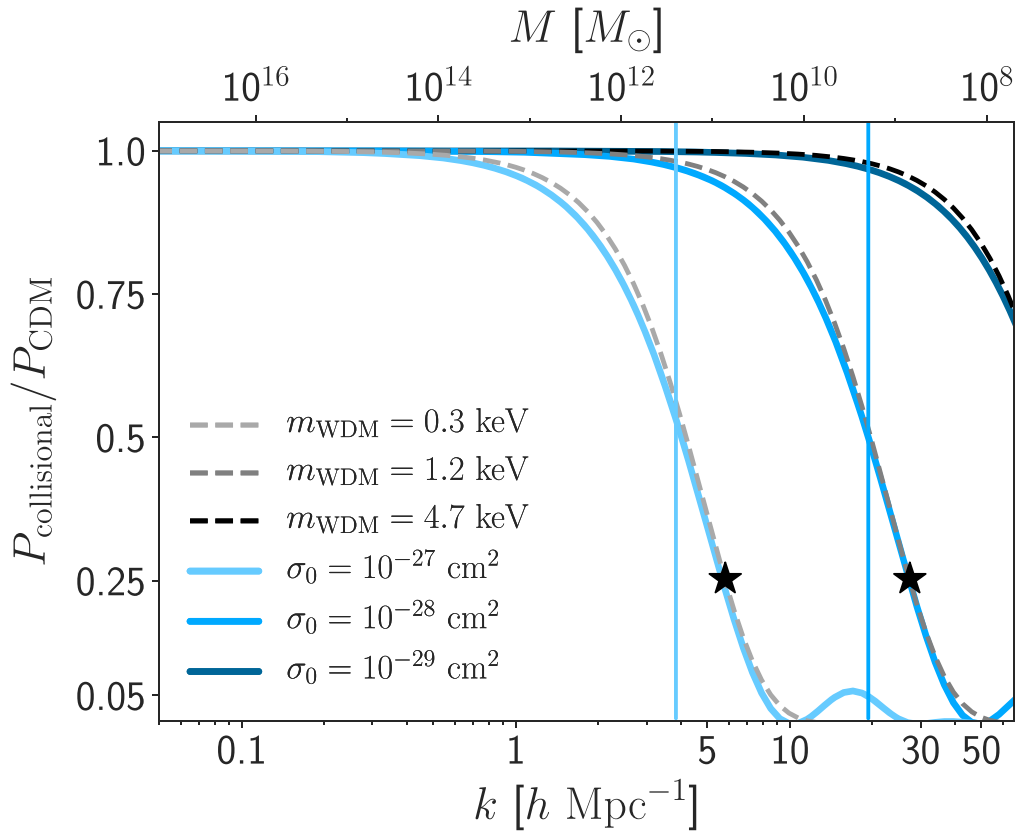
Figure 2. Ratio of the linear matter power spectrum in the presence of DM–baryon scattering relative to that in CDM (solid lines), for a range of interaction cross sections (for 1 MeV DM particles). Dashed lines show the same quantity for thermal relic warm DM models with matching half-mode scales (denoted as black stars). Vertical lines indicate the critical scale returned by our analytic minimum halo mass estimate.

suppressed scale along the cutoff in the linear matter power spectrum. We illustrate this in Figure 2, which shows transfer functions for the same σ_0 and m_χ values plotted in Figure 2 of N19. Rather than corresponding to a scale at which power is extremely suppressed relative to cold, collisionless DM (CDM)—i.e., ~1% in N19—the analytic estimate now lies at ~50% power suppression. As such, the analytic estimate is not as conservative as suggested by the original comparison to spuriously suppressed transfer functions. However, we emphasize that the analytic estimate was *not* designed to correspond to a particular level of power suppression, but rather to identify—in an order-of-magnitude sense—the scale at which the cutoff in the interacting DM transfer function occurs. Its purpose thus remains as interpreted in N19.

ORCID iDs

Ethan O. Nadler ⬤ https://orcid.org/0000-0002-1182-3825
Vera Gluscevic ⬤ https://orcid.org/0000-0002-3589-8637
Kimberly K. Boddy ⬤ https://orcid.org/0000-0003-1928-4667
Risa H. Wechsler ⬤ https://orcid.org/0000-0003-2229-011X

References

Angloher, G., Bauer, P., Bento, A., et al. 2017, EPJC, 77, 637
Aprile, E., Aalbers, J., Agostini, F., et al. 2017, PhRvL, 119, 181301
Bhoonah, A., Bramante, J., Elahi, F., & Schon, S. 2018, PhRvL, 121, 131101
Boddy, K. K., & Gluscevic, V. 2018, PhRvD, 98, 083510
Bringmann, T., & Pospelov, M. 2019, PhRvL, 122, 171801
Emken, T., & Kouvaris, C. 2018, PhRvD, 97, 115047
Erickcek, A. L., Steinhardt, P. J., McCammon, D., & McGuire, P. C. 2007, PhRvD, 76, 042007

Gluscevic, V., & Boddy, K. K. 2018, PhRvL, 121, 081301
Nadler, E. O., Gluscevic, V., Boddy, K. K., & Wechsler, R. H. 2019, ApJL, 878, L32
Petricca, F., Angloher, G., Bauer, P., et al. 2020, JPhCS, 1342, 012076
Wadekar, D., & Farrar, G. R. 2019, arXiv:1903.12190
Xu, W. L., Dvorkin, C., & Chael, A. 2018, PhRvD, 97, 103530